Received: 3 June 2021 | Revised: 6 November 2021 | Accepted: 8 November 2021

DOI: 10.1002/nbm.4658

RESEARCH ARTICLE

NMR IN BIOMEDICINE WILEY

High-resolution pH imaging using ratiometric chemical exchange saturation transfer combined with biosensor imaging of redundant deviation in shifts featuring paramagnetic DOTA-tetraglycinate agents

Jelena M. Mihailovic[1,2] | Yuegao Huang[1,2] | John J. Walsh[2,3] | Muhammad H. Khan[2,3] | Sandeep K. Mishra[1,2] | Sara Samuels[2] | Fahmeed Hyder[1,2,3] | Daniel Coman[1,2]

[1]Department of Radiology and Biomedical Imaging, Yale University, New Haven, Connecticut, USA

[2]Magnetic Resonance Research Center, Yale University, New Haven, Connecticut, USA

[3]Department of Biomedical Engineering, Yale University, New Haven, Connecticut, USA

Correspondence
Jelena M. Mihailovic and Fahmeed Hyder, Department of Radiology and Biomedical Imaging, Yale University, New Haven, N144 TAC (MRRC), 300 Cedar Street, CT 06520, USA.
Email: jelena.mihailovic@yale.edu and
Email: fahmeed.hyder@yale.edu

Funding information
NIH, Grant/Award Number: R01 EB-023366

Chemical exchange saturation transfer (CEST) and biosensor imaging of redundant deviation in shifts (BIRDS) methods differ respectively by detecting exchangeable and nonexchangeable proton signals by magnetic resonance. Because CEST contrast depends on both temperature and pH, simultaneous CEST and BIRDS imaging can be employed to separate these contributions. Here, we test if high-resolution pH imaging in vivo is possible with ratiometric CEST calibrated for temperature variations measured by BIRDS. Thulium- and europium-based DOTA-tetraglycinate agents, TmDOTA-$(gly)_4^-$ and EuDOTA-$(gly)_4^-$, were used for high-resolution pH mapping in vitro and in vivo, using BIRDS for temperature adjustments needed for a more accurate ratiometric CEST approach. Although neither agent showed pH dependence with BIRDS in vitro in the pH range 6 to 8, each one's temperature sensitivity was enhanced when mixed because of increased redundancy. By contrast, the CEST signal of each agent was affected by the presence of the other agent in vitro. However, pH could be measured more accurately when temperature from BIRDS was detected. These in vitro calibrations with TmDOTA-$(gly)_4^-$ and EuDOTA-$(gly)_4^-$ enabled high-resolution pH imaging of glioblastoma in rat brains. It was concluded that temperature mapping with BIRDS can calibrate the ratiometric CEST signal from a cocktail of TmDOTA-$(gly)_4^-$ and EuDOTA-$(gly)_4^-$ agents to provide temperature-independent absolute pH imaging in vivo.

KEYWORDS
aerobic glycolysis, electrolyte imbalance, glioblastoma, hepatocellular carcinoma, pH mapping, tumor microenvironment

Abbreviations used: BIRDS, biosensor imaging of redundant deviation in shifts; CEST, chemical exchange saturation transfer; CSI, chemical shift imaging; $DOTA^{4-}$, 1,4,7,10-tetraazacyclododecane-1,4,7,10-tetraacetate; DOTA-4AmP^{5-}, 1,4,7,10-tetraazacyclododecane-1,4,7,10-tetraaminophosphonate; $DOTMA^4$, 1,4,7,10-tetraazacyclododecane-tetramethyl-1,4,7,10-tetraacetate; RMSD, root-mean-square-deviation; TME, tumor microenvironment.

1 | INTRODUCTION

Magnetic resonance imaging (MRI) is widely used in diagnostic medicine and research because of its noninvasive nature and exquisite spatial resolution. MRI contrast relies mainly on the differences in proton density and relaxation properties of the water signal between different tissues. The intrinsic contrast can be improved further by enhancing relaxation with paramagnetic agents.[1,2] However, despite the success of gadolinium-based agents in clinical MRI, the contrast is always "on" when the agent is present, and the approach lacks molecular imaging specificity.

A novel class of contrast agents that uses the chemical exchange saturation transfer (CEST) effect has become available in the last few decades,[3,4] where the exchange of bulk water protons with hydroxyl/amine/amide protons on the agent is dependent on pH, temperature, and agent concentration. Paramagnetic CEST (PARACEST) agents have also been developed, where the chemical shifts of exchangeable protons are pushed farther away from the bulk water proton signal by paramagnetic lanthanide (III) complexes, containing thulium (Tm^{3+}) or europium (Eu^{3+}), or by transition (II) metal complexes to improve specificity.[3,5] An additional reason for using PARACEST agents with relatively large chemical shifts is that the CEST effect is observable only when the chemical shift difference (in Hz) between the two exchanging pools is greater than the proton exchange rate, allowing the usage of contrast agents with relatively fast exchange rates. Such lanthanide-based PARACEST agents are commonly used for molecular imaging,[6,7] because the chemical shift separation between their exchangeable pools is large (from tens to hundreds of ppm), and thus effects from direct saturation of the bulk water pool and magnetization transfer are negligible.[7,8] In addition, the large chemical shift difference between the exchanging pools provides the opportunity to use multiple PARACEST agents without signal overlap. This idea has been previously used to provide a concentration-independent pH readout using ratiometric CEST.[9–11] However, in these studies the temperature effects on the ratiometric CEST were not considered. Separation of temperature effects from other factors that affect the CEST signals (especially when using multiple agents) can significantly improve the accuracy of CEST-based measurements (like pH imaging). Furthermore, the CEST signals measured when using multiple paramagnetic agents are not a linear combination of their individual CEST signals,[12] due to the interdependence and nonlinearity of the chemical exchange effects when dealing with several exchanging pools.

In addition to the exchangeable protons of PARACEST agents, the nonexchangeable proton resonances emanating from the same agents could be utilized by biosensor imaging of redundant deviation in shifts (BIRDS) to generate temperature and/or pH maps using 3D chemical shift imaging (CSI).[13,14] The BIRDS method combines the high spatial resolution of MRI with the high molecular specificity of magnetic resonance spectroscopy (MRS), where paramagnetically shifted nonexchangeable protons (i.e. $-CH_y$) of macrocyclic complexes are directly detected.[13–19] Reduced (i.e. millisecond range) longitudinal (T_1) and transverse (T_2) relaxation times of nonexchangeable protons of BIRDS agents allow high-resolution and high-speed CSI.[13] The readout of the physicochemical environment does not depend on diffusion or blood flow, and BIRDS signals can be detected beyond MRI contrast (i.e. we see BIRDS signals even where the MRI images are darkened by T_2 shortening).[13,14,16,17] Moreover, although the distribution of BIRDS agents may depend on vessel permeability (e.g. normal vs. tumor tissue), the shift-based reporting is independent of the agent's dose. Various paramagnetic BIRDS agents have been applied to map temperature[17,20] or pH in vivo.[21] Dual CEST and BIRDS imaging capabilities were demonstrated using the Eu^{3+} salt of 1,4,7,10-tetraazacyclododecane-1,4,7,10-tetraacetate ($DOTA^{4-}$) tetraglycinate (EuDOTA-$(gly)_4^-$).[15] Measured CEST properties of EuDOTA-$(gly)_4^-$ are manifested by proton exchange between bulk water and bound water pools. The remaining proton signals emanating from the backbone of the $DOTA^{4-}$ chelate do not exchange and therefore are readily detectable by conventional ^1H MRS and BIRDS. A variation in pH has little effect on the chemical shifts of these protons. EuDOTA-$(gly)_4^-$ was used to demonstrate that its CEST characteristics are preserved, while BIRDS properties are detected. The temperature sensitivity of EuDOTA-$(gly)_4^-$ was used to show that qualitative MR contrast with CEST can be calibrated using quantitative MR mapping with BIRDS, thereby enabling quantitative molecular imaging at high spatial resolution. More recently, BIRDS with DOTA-based phosphonates, the Tm^{3+} and ytterbium (Yb^{3+}) salts of $DOTA^{4-}$ tetraglycinate (i.e. TmDOTA-4AmP^{5-} and YbDOTA-4AmP^{5-}, respectively), has been proposed to calibrate the quantification of the PARACEST properties of these agents.[18] The DOTA-4AmP^{8-} chelate contains nonexchangeable protons, exchangeable protons, and phosphonate groups, imparting pH-sensing capabilities when chelated with Tm^{3+} and Yb^{3+}. BIRDS and CEST experiments have shown that both complexes are responsive to pH and temperature changes. Higher pH and temperature sensitivities are obtained with BIRDS for each complex when using the chemical shift difference between two proton resonances compared with using the chemical shift of a single proton resonance, thereby eliminating the need to use the water resonance as a reference. Based on these results and inspired by the high temperature sensitivity in the Tm^{3+} complex of 1,4,7,10-tetramethylcyclen-1,4,7,10-tetraacetate ($DOTMA^{4-}$), $TmDOTMA^{-}$[14] and dual BIRDS/PARACEST properties in TmDOTA-4AmP^{5-}[14] probes that have several nonexchangeable groups at the same or different positions (for BIRDS) and exchangeable protons (for PARACEST), we propose in this study to use a mixture of TmDOTA-$(gly)_4^-$ and EuDOTA-$(gly)_4^-$ for dual BIRDS/PARACEST detection. We hypothesize that the nonexchangeable protons in the mixture would provide both higher temperature sensitivity and more redundancy for BIRDS imaging, while exchangeable protons (i.e. amide groups) would provide opportunities for pH imaging with quantitative PARACEST analysis.

The maintenance of pH homeostasis in the brain is of key importance for the proper execution of neurotransmission, and deviations from this homeostasis are a crucial factor in the mechanism underlying a spectrum of pathological conditions. It is widely accepted that the extracellular pH (pH_e) in cancers is lower than in normal tissue.[22] Generally, pH_e values in normal tissues (brain, subcutaneous tissues, etc.) are in the range of 7.2–7.5. However, the pH_e of tumor cells is mildly acidic in the range of 6.4–7.0. Warburg[23] reported increased aerobic glycolysis in hens with Rouse sarcoma and showed decreased glucose and increased lactic acid concentrations in the axillary veins on the tumor side compared with the normal

side. Subsequently, researchers have investigated the mechanisms of pH control in the tumor microenvironment (TME). Novel strategies have been developed to control the pH_e in the TME to induce apoptosis of cancer cells, improving treatment efficiency. Thus, there is an increased need for more accurate pH-imaging techniques at higher resolution.[24,25]

pH imaging using paramagnetic MRI contrast agents was shown before with either ratiometric CEST[26] or just BIRDS.[14,15] Although pH imaging is possible using ratiometric PARACEST, its accuracy is affected by potential variations in the tissue temperature. However, the accuracy of pH measurements using ratiometric PARACEST can be improved by correcting for temperature effects measured with BIRDS. In the present work, we show that BIRDS properties are retained after mixing two paramagnetic agents, TmDOTA-$(gly)_4^-$ and EuDOTA-$(gly)_4^-$. Moreover, the temperature sensitivity is enhanced because of added redundancy when using the most sensitive signals from each agent. These two agents are good candidates for dual BIRDS and CEST imaging because their proton spectra span a wide range of frequencies, while their effect on water relaxation is minimal.[27]

2 | MATERIALS AND METHODS

2.1 | Sample preparation

TmDOTA-$(gly)_4^-$ and EuDOTA-$(gly)_4^-$ (Figure 1A,B) were purchased from Macrocyclics (Dallas, TX). The synthesis of these two agents was described by Aime et al.[9] The 10 mM TmDOTA-$(gly)_4^-$ and 10 mM EuDOTA-$(gly)_4^-$ samples, and mixtures of 10 mM TmDOTA-$(gly)_4^-$ and 10 mM EuDOTA-$(gly)_4^-$, were prepared in 10 mM phosphate buffer at various pH values (6.4–7.9) with 10% D_2O (CAS no. 7789-20-0; Sigma-Aldrich, St. Louis, MO) for the BIRDS and CEST experiments.

2.2 | ^{1}H MRS for paramagnetic BIRDS calibration

^{1}H spectra for TmDOTA-$(gly)_4^-$ and EuDOTA-$(gly)_4^-$, and the mixture samples (pH 6.4–7.9), were recorded on an 11.7-T vertical magnet (Bruker, Billerica, MA) with a TR of 100 ms at various temperatures ranging from 27 to 40°C. The temperature measurement was calibrated as described previously.[15] All spectra were line-broadened (20 Hz), phased and baseline-corrected. The proton resonances were assigned according to previous reports.[8,15] The chemical shifts of proton resonances were recorded relative to the water resonance (0 ppm). The H2 and H6 proton resonances of TmDOTA-$(gly)_4^-$, named Tm-H2 and Tm-H6, and the H4 resonance of EuDOTA-$(gly)_4^-$, named Eu-H4, were chosen for characterization with paramagnetic BIRDS. Given that the two complexes TmDOTA-$(gly)_4^-$ and EuDOTA-$(gly)_4^-$ do not show pH-sensitive peaks over the pH range of interest (6.4 to 7.9), the temperature (T) can be calculated from the chemical shift difference between the Tm-H2 (δ_{Tm-H2}) and Tm-H6 (δ_{Tm-H6}) resonances according to:

$$T_{TmDOTA-(gly)_4^-} = -1.36 \times (\delta_{Tm-H2} - \delta_{Tm-H6}) + 186.80, \quad (1)$$

providing a temperature sensitivity of -0.74 ppm/°C. The chemical shift of Eu-H4 (δ_{Eu-H4}) can also be used to determine the temperature according to:

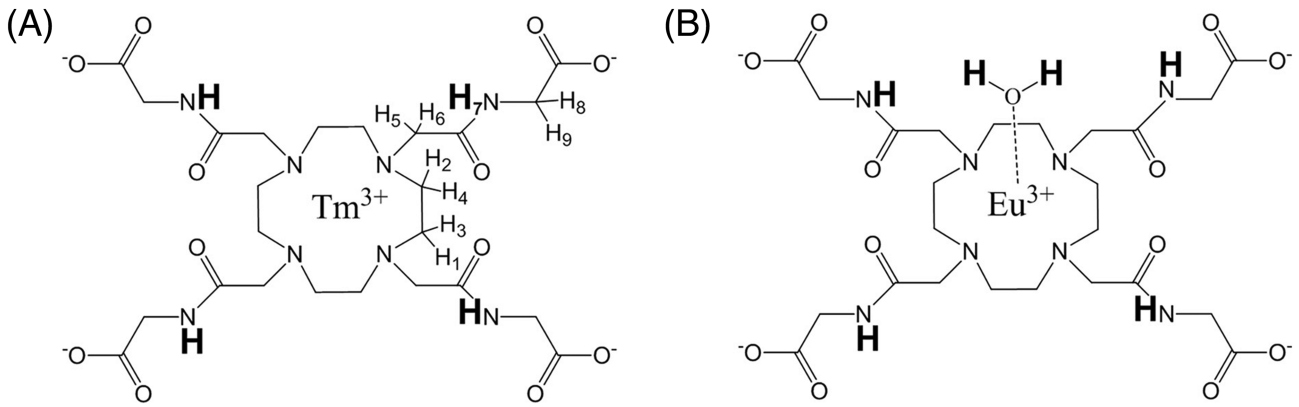

FIGURE 1 Chemical structures of the paramagnetic agents used. Both (A) TmDOTA-$(gly)_4^-$ and (B) EuDOTA-$(gly)_4^-$ have exchangeable (shown in bold) and nonexchangeable protons

$$T_{EuDOTA-(gly)_4^-} = -7.92 \times \delta_{Eu-H4} + 191.59, \quad (2)$$

providing a temperature sensitivity of −0.12 ppm/°C.

The T_1 and T_2 relaxation times for these resonances were measured at pH 7.4 and 35°C using standard inversion-recovery and spin-echo methods, respectively (Table 1).

2.3 | ^{1}H MRS for PARACEST calibration

All CEST experiments for TmDOTA-$(gly)_4^-$, EuDOTA-$(gly)_4^-$, and the mixture samples (pH ranges 6.4–7.9) were collected on an 11.7-T vertical magnet (Bruker) using a 4-s continuous wave saturation pulse (16.7 μT) over a ±100 ppm frequency range at 250 Hz/point, followed by a 7-μs excitation pulse to measure the bulk water signal at different temperatures (30–40°C). The CEST effect was quantified as a decrease in the bulk water intensity according to the following equation:

$$CEST = 1 - \frac{M_z}{M_0}, \quad (3)$$

where M_z is the water proton magnetization upon saturation at the frequency of interest and M_0 is the equilibrium magnetization.

2.4 | In vitro pH mapping with BIRDS and CEST

Separate samples (phantoms) containing 10 mM TmDOTA-$(gly)_4^-$ and 10 mM EuDOTA-$(gly)_4^-$ at different pH values (i.e. 6.43, 6.86, 7.13, 7.42, and 7.74) were prepared for demonstration of in vitro pH mapping at high resolution. Both 3D CSI data for BIRDS and CEST were obtained on a 11.7-T Bruker horizontal bore spectrometer (Bruker Avance system interfaced with Bruker ParaVision v. 6.0.1 software) using a volume birdcage radiofrequency (RF) coil (4-cm diameter) using a field of view of 32 × 32 mm. The 3D CSI was acquired with a repetition time (TR) of 10 ms and a 600-μs Gaussian pulse for excitation. The 3D CSI data were reconstructed to a 25 × 25 × 25 resolution. The MRI for CEST were acquired using a spin-echo sequence with a TR of 8 s, TE of 10 ms, and image matrix of 64 × 64. A continuous wave of 4 s was used for saturation of various frequencies in the range of −100 to +100 ppm. The temperature was controlled by circulating hot air at different temperatures around the phantoms in the magnet bore. The temperature was monitored by a thermocouple positioned next to the phantoms investigated. The pH imaging at high resolution was obtained from the temperature (T) measured with BIRDS and the ratiometric CEST (R) measured with CEST, according to the polynomial equation:

$$\begin{aligned} pH = a + b \cdot R + c \cdot T + d \cdot R^2 + e \cdot T^2 + f \cdot R \cdot T + g \cdot R^3 + h \cdot T^3 \\ + i \cdot R \cdot T^2 + j \cdot R^2 \cdot T, \end{aligned} \quad (4)$$

where the coefficients a-j (Table 2) were calculated from the nonlinear fit of pH as a function of T and R.

TABLE 1 Temperature sensitivities and relaxation times for selected protons of paramagnetic agents in BIRDS

	Tm-H2		Tm-H6		Eu-H4	
	$TmDOTAgly_4^-$	Mixture	$TmDOTAgly_4^-$	Mixture	$EuDOTAgly_4^-$	Mixture
C_T (ppm/°C)[a]	−0.251 ± 0.001	−0.251 ± 0.001	0.478 ± 0.002	0.476 ± 0.002	−0.123 ± 0.001	−0.125 ± 0.001
T_1 (ms)[b]	2.27 ± 0.02	2.24 ± 0.02	2.79 ± 0.02	2.70 ± 0.02	13.3 ± 0.7	11.7 ± 0.5
T_2 (ms)[b]	1.70 ± 0.03	1.61 ± 0.05	2.56 ± 0.09	2.22 ± 0.06	5.5 ± 0.1	5.8 ± 0.2

[a]Average temperature sensitivities for all measured samples at 11.7 T.
[b]Measurements are accomplished for 10 mM samples at 35°C, pH 7.4, and 11.7 T.

TABLE 2 Coefficents for pH calculation using ratiometric PARACEST from the CEST ratio and temperature in mixture

a	b	c	d	e	f	g	h	i	j	r^2
10.98	4.96	−0.41	−0.0054	0.12	−0.21	0.075	−0.00014	0.0032	−0.014	0.98

Additional phantoms containing 10 mM TmDOTA-$(gly)_4^-$ at pH 7.40, 10 mM EuDOTA-$(gly)_4^-$ at pH 7.40, and a mixture of 10 mM TmDOTA-$(gly)_4^-$ and 10 mM EuDOTA-$(gly)_4^-$ at pH 7.41, were prepared for validation of in vitro pH measurements. Moreover, for validation purposes, individual and mixture phantoms of 10 mM TmDOTA-$(gly)_4^-$ and 10 mM EuDOTA-$(gly)_4^-$ with unknown pH were prepared. The pH-mapping capability at low agent concentrations was also demonstrated using mixture phantoms containing 1 mM TmDOTA-$(gly)_4^-$ and 1 mM EuDOTA-$(gly)_4^-$ at pH 6.8 and 7.5, at 30 and 37°C. The BIRDS and CEST data for these phantoms were obtained using the same pulse sequences and parameters as described above.

2.5 | In vivo pH mapping with BIRDS and CEST

All animal procedures were approved by the Institutional Animal Care and Use Committee (IACUC) at Yale University (protocol 11,634). The Fischer 344 rats (200–250 g, n = 3) were implanted with 1.25×10^3 RG2 glioma cells as previously described.[21] The rats were anesthetized with isoflurane (2%–3%) and positioned in a stereotaxic instrument with the incisor bar set at 3.0 mm below the interaural line. RG2 cells at high confluence were harvested, washed, and suspended in appropriate media. Intracranial injections were made with a 25-μL Hamilton syringe fitted with a 26-gauge beveled needle, into the right cortex 3 mm to the right from bregma and 3 mm ventral to the dura. A 5-μL volume of the cell suspension was injected over the course of 5 min and the needle was left in place for an additional 5 min before slow withdrawing. After injection, the scalp was closed, treated with antibiotic, and a nonsteroidal anti-inflammatory drug (meloxicam, 1 mg/kg) was injected subcutaneously to prevent pain and inflammation. Tumor growth was monitored every 3–4 days using ^{1}H-MRI. The animals were imaged when the tumors reached a diameter larger than 3 mm, at ~15–18 days postinjection. On the day of the scanning, the rats were anesthetized with isoflurane (<2%) and a mixture of 70% N_2O/30% O_2. Because body temperature decreases in animals under anesthesia, a water-heating pad was used to maintain the body temperature in the physiological range (36–37°C). The body temperature was measured with a rectal temperature probe. We did not observe any significant temperature increases due to RF fields applied through RF coils during the experiments. A tail vein catheter was used for injection of the TmDOTA-$(gly)_4^-$ and EuDOTA-$(gly)_4^-$ mixture at a rate of 1 mmol/kg/h for ~1 h. The BIRDS and CEST data in rat brain were obtained using the same pulse sequences and parameters as described above for the in vitro experiments. The head position was adjusted using gradient-echo (GE) fast low angle shot magnetic resonance imaging (FLASH). Second order shim was applied after B_0 mapping using GE. Before/after the infusion of paramagnetic contrast agents, anatomical T_2-weighted images were obtained using a spin-echo sequence with 10 axial slices (FOV: 25×25 mm^3, 128×128 in-plane resolution) and 10 echo times; TE = 10–100 ms, TR = 4 s. The 1-mm single-slice CEST MRI data were acquired using a 2D spin-echo EPI sequence with a TR of 6000 ms, TE of 10 ms with FOV of 25×25 mm^2 and image matrix of 64×64. A continuous wave of 4 s was used for saturation of various frequencies in the range of −100 to +100 ppm. For B_0 corrections, water saturation shift-referencing (WASSR) images were acquired, an RF saturation power of 0.2 μT and pulse length of 2 s. Before the CEST experiment, a single-slice B_1 field map was created using a two flip angle-imaging approach (T_R = 10,000 ms, T_E = 6 ms, flip angles 60° and 120°, 1 average, FOV = 25×25 mm^2 and matrix size 42×42, acquisition time of ~5.26 min each). One CEST dataset and several BIRDS (CSI) datasets were acquired for 2 h starting at 30 min after the start of the infusion. BIRDS data were acquired using a surface RF coil (14-mm diameter), while all the other MR data including CEST-related acquisitions were obtained with a birdcage RF coil (40-mm diameter). The 3D CSI for BIRDS was performed using a dual-band Shinnar-Le Roux pulse with an excitation bandwidth of 42 kHz and 204-μs pulse duration, T_R = 7 ms and FOV of $25 \times 25 \times 25$ mm^3. The 3D spherical encoding was obtained with 160-μs phase-encoding gradients. A total of 120 averages were acquired for each MRS dataset for a total scan duration of ~30 min. The total MR session time was 3 to 4 h. The spectrum in each voxel was line-broadened (500 Hz), phased (first order) and baseline-corrected. The SNR for the peak of interest was calculated from "signal" and "noise" measurements

$$\mathrm{SNR} = \frac{\mathrm{signal}}{\mathrm{noise}}, \tag{5}$$

where the "signal" was defined as the height of the Lorentzian fitted peak and the "noise" as the mean signal in a spectral region containing no resonances.

To quantify R, T, and pH error maps, defined as the deviation from the predicted model (Equations 1–4), we applied the root-mean-square-deviation (RMSD) method. Detailed information about this method can be found elsewhere.[28] Briefly, the RMSD is a measure of the difference between values predicted by a model and the values observed from the data and is given by:

$$RMSD = \sqrt{\sum_{i=1}^{n} \frac{\hat{\theta}^2}{n}} - \sqrt{\sum_{i=1}^{n} \frac{\theta^2}{n}}, \tag{6}$$

where $\widehat{\theta}_{1....n}$ are the values predicted by the model, $\theta_{1...n}$ the observed values, and n is the number of observations (see the supporting information, Appendix). The errors in R, T, and pH were obtained pixel-wise. All data analysis was performed using an in-house written code in MATLAB (MathWorks, Natick, MA).

3 | RESULTS

^{1}H spectra of individual TmDOTA-(gly)$_4^-$ (Figure 2A) and EuDOTA-(gly)$_4^-$ (Figure 2B) samples, and of their mixture (Figure 2C), show hyperfine shifts characteristic to nonexchangeable proton resonances of paramagnetic complexes.[13,15] The ^{1}H spectrum of the mixture shows no differences in chemical shifts compared with those of individual TmDOTA-(gly)$_4^-$ and EuDOTA-(gly)$_4^-$ spectra, indicating that BIRDS signals of either agent are not affected by the presence of the other agent. The temperature sensitivities of Tm-H2, Tm-H6, and Eu-H4 resonances (Figure 2) are in the range of 0.12 to 0.48 ppm/^{0}C (Table 1) and are the largest among all the nonexchangeable protons. Although Eu-H4 has the smallest temperature sensitivity, −0.123 ppm/°C in the individual sample and −0.125 ppm/°C in the mixture, this peak can still be solely used for accurate temperature mapping, as we have shown previously.[15] There was no significant difference between the temperature sensitivities in the individual samples compared with those in the mixture (Table 1). Moreover, a negligible chemical shift dependence on pH was observed for these three protons in the pH range investigated (6.4–7.9).

The Tm-H2, Tm-H6, and Eu-H4 resonances were well separated from other proton resonances and they displayed high sensitivity, which remained unchanged after mixing the two agents (Figure 2). The T_1 values of Tm-H2 and Tm-H6 protons are 2.27 ± 0.02 and 2.79 ± 0.02 ms, respectively, in the individual samples, and they also did not change significantly after mixing the two agents (Figure S1A,B,D,E and Table 1). The T_1 of Eu-H4 is 13.3 ± 0.7 ms in the individual EuDOTA-(gly)$_4^-$ sample, and slightly decreases to 11.7 ± 0.5 ms in the mixture (Figure S1C,F and Table 1). The T_2 of Tm-H2 and Tm-H6 protons are 1.70 ± 0.03 and 2.56 ± 0.09 ms, respectively, in the individual samples, and they decrease slightly to 1.61 ± 0.05 and 2.22 ± 0.06 ms, respectively, after mixing the two agents (Figure S1A,B,D,E and Table 1). The T_2 for Eu-H4 is 5.5

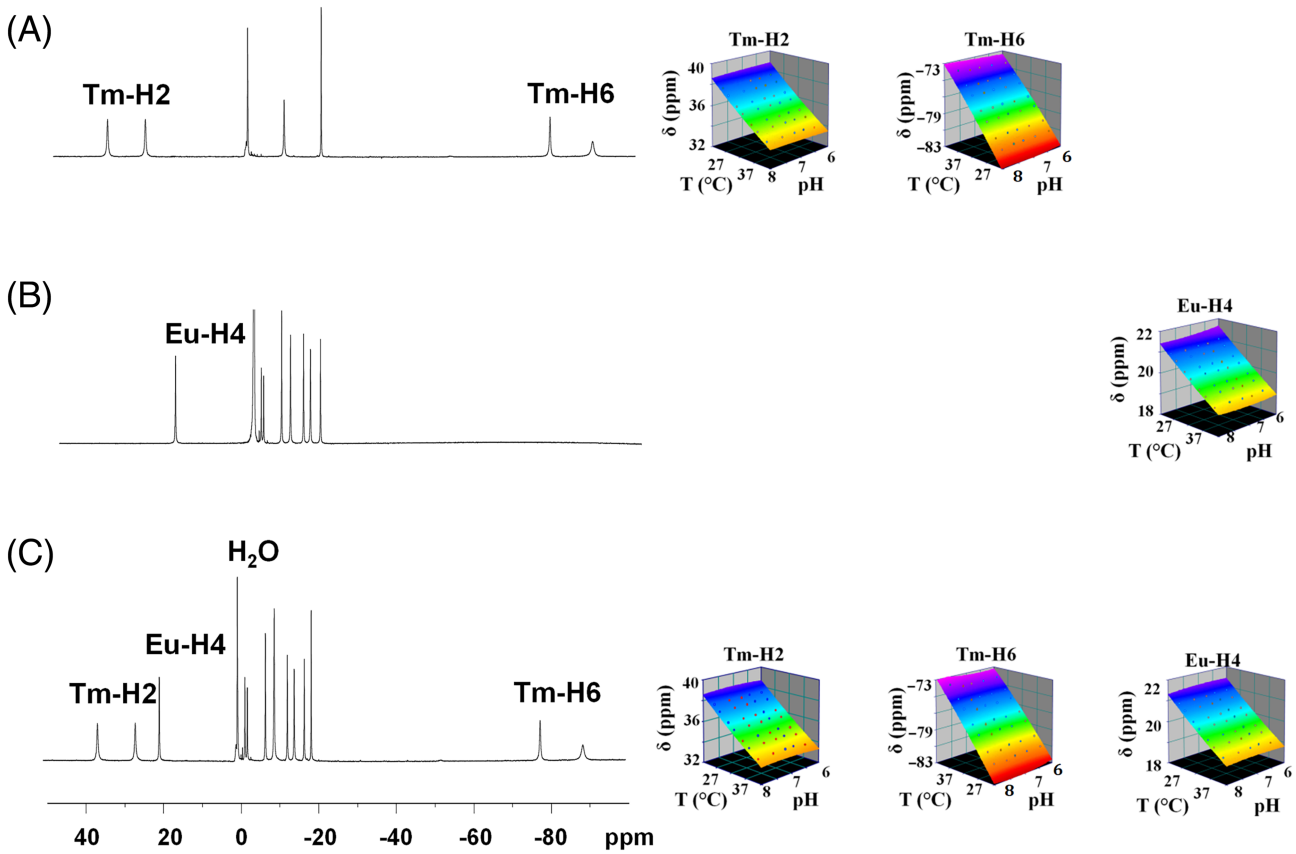

FIGURE 2 ^{1}H spectra and BIRDS characterization of the paramagnetic agents (A) TmDOTA-(gly)$_4^-$, (B) EuDOTA-(gly)$_4^-$, and (C) the mixture of TmDOTA-(gly)$_4^-$ and EuDOTA-(gly)$_4^-$ at 11.7 T, 35°C, and pH 7.4 (10 mM each). The proton resonances used for BIRDS are labeled, and temperature/pH dependencies are shown as 3D surface plots

± 0.1 ms in the individual EuDOTA-$(gly)_4^-$ sample and 5.8 ± 0.2 ms in the mixture (Figure S1C,F and Table 1). The short relaxation times of these three protons combined with their high sensitivity makes them the best candidates for temperature sensing with BIRDS.

Both TmDOTA-$(gly)_4^-$ and EuDOTA-$(gly)_4^-$ have exchangeable protons and thus can also be used as PARACEST agents.[9,29] We acquired the Z-spectra for TmDOTA-$(gly)_4^-$ and EuDOTA-$(gly)_4^-$ independently, and for their mixture at various pH and temperature values (Figure 3). At 35°C, the amide protons of TmDOTA-$(gly)_4^-$ resonate at −52.5 ppm, while the bound water protons in EuDOTA-$(gly)_4^-$ resonate at 51.5 ppm (Figure 3A,B). The chemical shifts of these two exchangeable pools remain unchanged after mixing the two agents (Figure 3C). The CEST effect for the TmDOTA-(gly) increases as the pH increases (Figure 3A), while for EuDOTA-$(gly)_4^-$ the pH effect is much smaller (Figure 3B). In the mixture, the pH has a similar effect to that observed in individual solutions (Figure 3C). However, the amplitude of the CEST effect for the bound water proton pool of EuDOTA-$(gly)_4^-$ is significantly attenuated in the mixture (Figure 3B,C).

Changing the temperature of either TmDOTA-$(gly)_4^-$ or EuDOTA-$(gly)_4^-$ samples affects both the chemical shift and the amplitude of the CEST effect (Figure 3D-F). Increasing the temperature from 30 to 40°C shifts the CEST peaks toward the water resonance. We measured temperature sensitivities of 0.35 and −0.39 ppm/°C for the amide protons in TmDOTA-$(gly)_4^-$ (Figure 3D) and the bound water in EuDOTA-$(gly)_4^-$ (Figure 3E), respectively; the same temperature sensitivities were measured in the mixture (Figure 3F). Interestingly, in TmDOTA-$(gly)_4^-$, the CEST amplitude increases with temperature, while in EuDOTA-$(gly)_4^-$ the CEST amplitude decreases and becomes wider, a trend which was also observed in the mixture (Figure 3D-F).

To better compare the temperature sensitivities of various TmDOTA-$(gly)_4^-$ and EuDOTA-$(gly)_4^-$ proton resonances in individual solutions with those in the mixture, we plotted these sensitivities against each other (Figure 4A). The linear fit has a slope of 1.003, indicating that the temperature sensitivities are not affected by the presence of the other agent in the mixture. A similar comparison between the individual solutions and the mixture was performed for the CEST amplitude (Figure 4B). In this case we observed that for the TmDOTA-$(gly)_4^-$ the slope was close to unity, while for EuDOTA-$(gly)_4^-$ the slope deviated significantly from unity, indicating that the CEST intensities in the mixture are affected by the presence of other CEST agents with chemical exchangeable pools.

To demonstrate the capability of BIRDS to image temperature using various nonexchangeable proton resonances we used five samples containing a mixture of TmDOTA-$(gly)_4^-$ and EuDOTA-$(gly)_4^-$ with pH in the range of 6.4 to 7.8. The ambient temperature was set to six different values in the range of 23–40°C (Figure 5). The temperature maps were calculated with either Tm-H2 or Tm-H6 of TmDOTA-$(gly)_4^-$ using Equation 1 (Figure 5A-F), or Eu-H4 of EuDOTA-$(gly)_4^-$ using Equation 2 (Figure 5G-L). In addition, temperature maps were calculated by averaging the temperature maps generated individually using the TmDOTA-$(gly)_4^-$ or EuDOTA-$(gly)_4^-$ signals (Figure 5M-R). Similarly, maps of CEST amplitudes

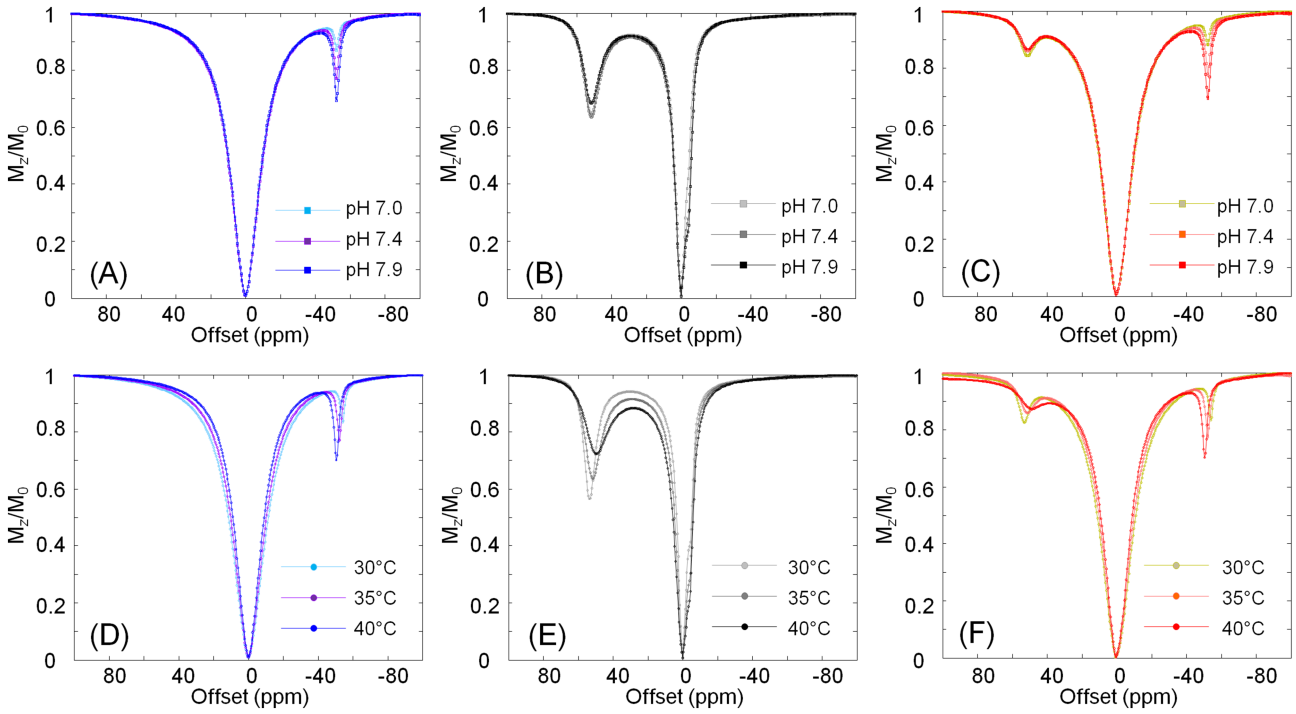

FIGURE 3 Z-spectra demonstrating CEST characterization of the paramagnetic agents (A and D) TmDOTA-$(gly)_4^-$, (B and E) EuDOTA-$(gly)_4^-$, and (C and F) the mixture of TmDOTA-$(gly)_4^-$ and EuDOTA-$(gly)_4^-$ at 11.7 T, 35°C, and pH 7.4 (10 mM each). The pH dependencies are shown at 35°C for (A) TmDOTA-$(gly)_4^-$, (B) EuDOTA-$(gly)_4^-$, and (C) the mixture of TmDOTA-$(gly)_4^-$ and EuDOTA-$(gly)_4^-$. The temperature dependence is shown at pH 7.4 for (D) TmDOTA-$(gly)_4^-$, (E) EuDOTA-$(gly)_4^-$, and (F) the mixture of TmDOTA-$(gly)_4^-$ and EuDOTA-$(gly)_4^-$

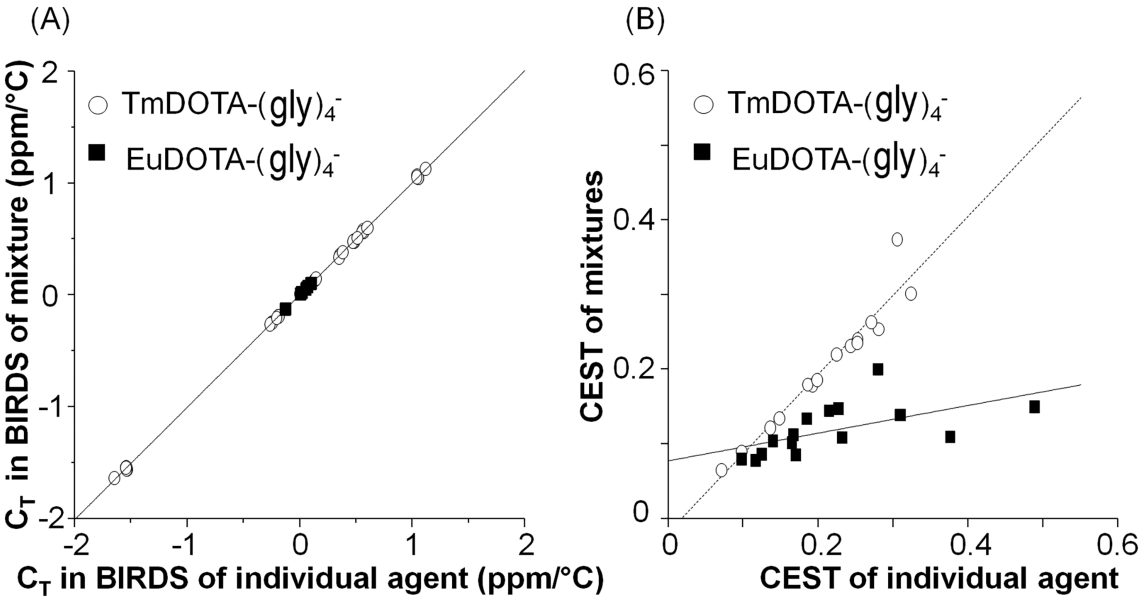

FIGURE 4 Comparison of temperature sensitivities (A) with BIRDS and (B) CEST amplitudes between samples containing the individual paramagnetic agents and an equimolar mixture of the two agents. The lines represent the least-square fit of the individual versus mixture sample measurements

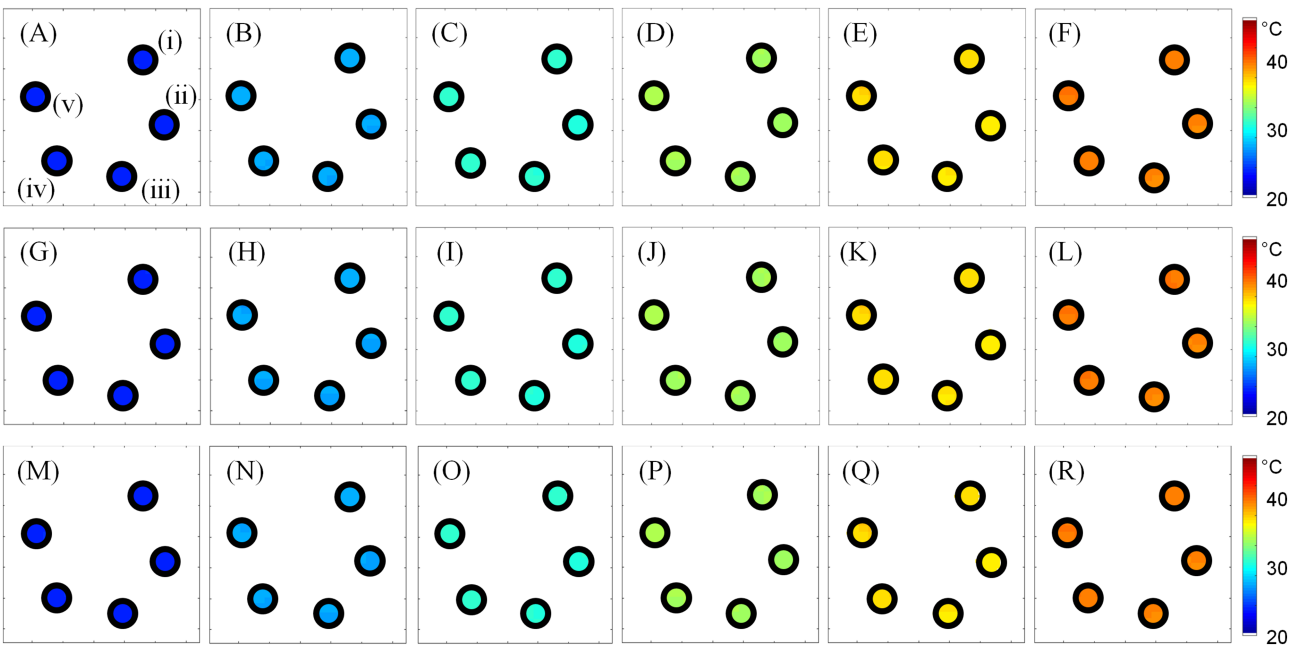

FIGURE 5 Temperature mapping with BIRDS for samples containing 10 mM TmDOTA-$(gly)_4^-$ and 10 mM EuDOTA-$(gly)_4^-$ at different pH and temperatures. The temperature was measured using the TmDOTA-$(gly)_4^-$ signals (A-F) and the EuDOTA-$(gly)_4^-$ signals (G-L) at different pH values (i: 6.43, ii: 6.86, iii: 7.13, iv: 7.42, v: 7.74) and different temperatures (A, G, M: 23.7°C; B, H, N: 27.0°C; C, I, O: 30.2°C; D, J, P: 33.2°C; E, K, Q: 36.1°C; F, L, R: 38.5°C). In addition, an average temperature map was also calculated from the individual temperature maps (M-R)

were generated at various temperatures in the range of 23–40°C using the amide proton in TmDOTA-$(gly)_4^-$ (Figure 6A-F) and the bound water in EuDOTA-$(gly)_4^-$ (Figure 6G-L). These two signals were then used to create ratiometric CEST maps at different temperatures (Figure 6M-R). These results demonstrate that the PARACEST ratio (named $CEST^{Tm/Eu}$) depends on both pH and temperature, and thus we can determine the pH by measuring the temperature with paramagnetic BIRDS and $CEST^{Tm/Eu}$ with PARACEST. The empirical relationship between pH, temperature, and $CEST^{Tm/Eu}$ (Figure 7) can be described by a polynomial equation (Equation 4).

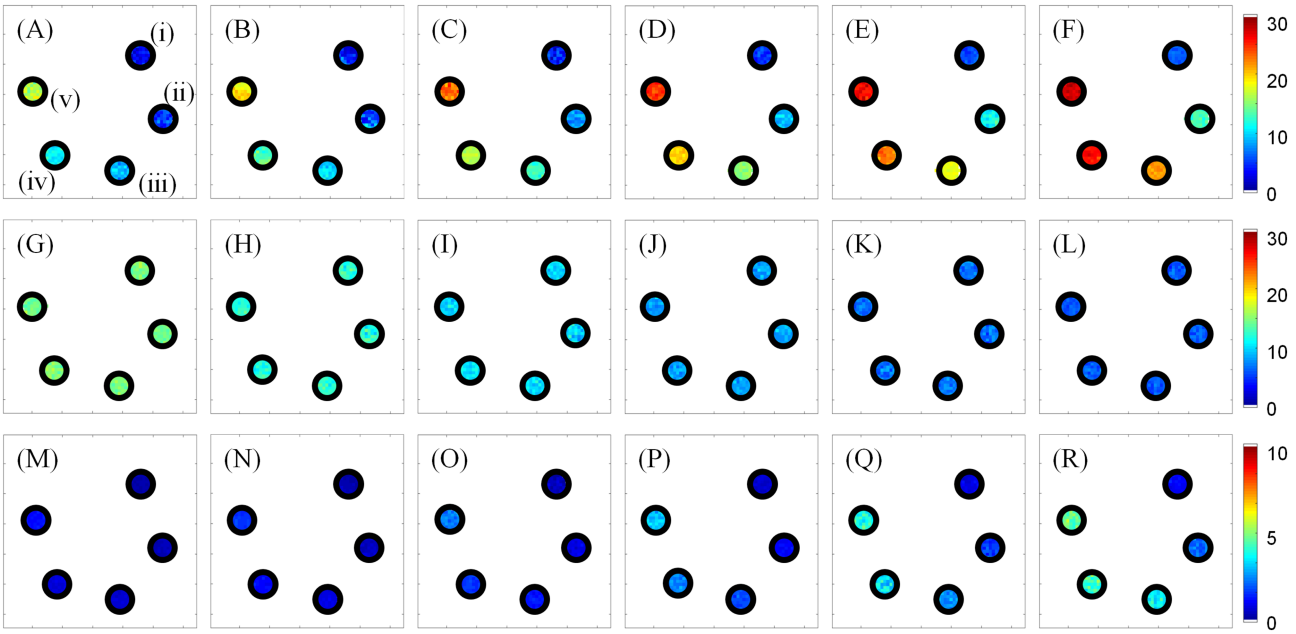

FIGURE 6 CEST imaging of TmDOTA-$(gly)_4^-$ (A-F) and EuDOTA-$(gly)_4^-$ (G-L), and ratiometric CEST of TmDOTA-$(gly)_4^-$ and EuDOTA-$(gly)_4^-$ (M-R) for mixtures containing 10 mM TmDOTA-$(gly)_4^-$ and 10 mM EuDOTA-$(gly)_4^-$ at different pH values (i: 6.43, ii: 6.86, iii: 7.13, iv: 7.42, v: 7.74) and different temperatures (A, G, F: 23.7°C; B, H, N: 27.0°C; C, I, O: 30.2°C; D, J, P: 33.2°C; E, K, Q: 36.1°C; F, L, R: 38.5°C)

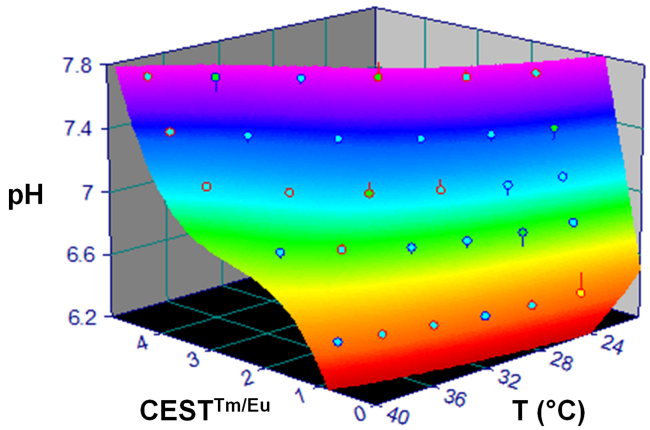

FIGURE 7 Model for measuring pH using the $CEST^{Tm/Eu}$ ratio (R) and temperature (T). The $CEST^{Tm/Eu}$ ratio R was obtained from the CEST intensities of amide protons in TmDOTA-$(gly)_4^-$ and the bound water in EuDOTA-$(gly)_4^-$. The temperature was determined from the chemical shift of H2 and H6 protons in TmDOTA-$(gly)_4^-$, and H4 proton in EuDOTA-$(gly)_4^-$ using BIRDS

To exemplify the measurement of pH in vitro using this approach, we prepared two samples containing the individual agents TmDOTA-$(gly)_4^-$ and EuDOTA-$(gly)_4^-$ at pH 7.40, and a sample containing a mixture of the two agents at pH 7.41 (Figure 8A). The BIRDS and CEST data were acquired at an ambient temperature of 33–34°C. We obtained the temperature maps of these samples from the Tm-H2 and Tm-H6 proton signals of TmDOTA-$(gly)_4^-$ using Equation 1 (Figure 8B), and from the Eu-H4 proton signal of EuDOTA-$(gly)_4^-$ using Equation 2 (Figure 8C). The calculated temperatures were very similar when using these two different measuring methods. The temperature map of the mixture sample was also determined by averaging the temperature values obtained using the signals from each agent individually (Figure 8D). We also generated CEST amplitude maps from each individual agent or the mixture samples using TmDOTA-$(gly)_4^-$ (Figure 8E) or EuDOTA-$(gly)_4^-$ (Figure 8F) signals, and we determined the $CEST^{Tm/Eu}$ map for the mixture (Figure 8G). Consistent with the results described in Figures 3 and 4, the CEST intensity of EuDOTA-$(gly)_4^-$ in the mixture is attenuated (Figure 8F), while the CEST intensity of TmDOTA-$(gly)_4^-$ in the mixture is similar (Figure 8E) when compared with those of individual agent samples. Using the temperature (33.4 ± 0.2°C) calculated in Figure 8D and $CEST^{Tm/Eu}$ (2.35 ± 0.03) obtained in Figure 8G, we created the corresponding pH map (Figure 8H) according to Equation 4 and calculated an average pH of 7.43 ± 0.04 in the mixture sample. This value is in excellent agreement with the value of 7.41 measured with a pH electrode in the mixture sample. To

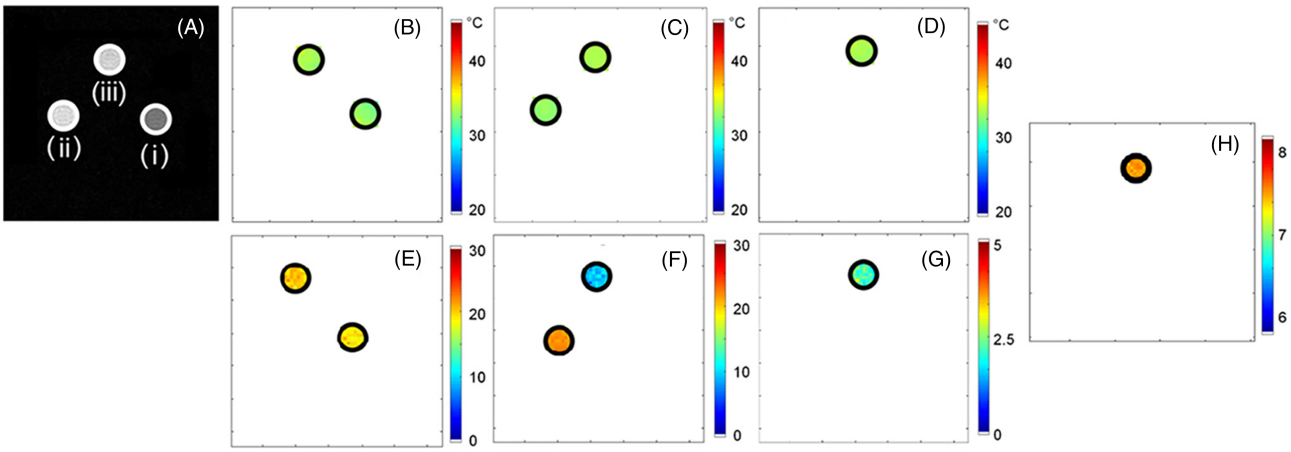

FIGURE 8 In vitro validation of pH measurements in a phantom containing three samples. (A) Phantom orientation of (i) 10 mM EuDOTA-$(gly)_4^-$ at pH 7.40; (ii) 10 mM TmDOTA-$(gly)_4^-$ at pH 7.40; and (iii) 10 mM TmDOTA-$(gly)_4^-$ and 10 mM EuDOTA-$(gly)_4^-$ at pH 7.41. The temperature was measured using BIRDS (B-D), while the CEST ratio (E-G) was obtained using CEST. The pH map (H) was obtained from the $CEST^{Tm/Eu}$ ratio R (G) and temperature (D) using Equation 4

demonstrate that this high-resolution pH-mapping method is independent of the concentration of the two agents and can be used at lower concentrations, we used two mixture samples containing 1 mM TmDOTA-$(gly)_4^-$ and 1 mM EuDOTA-$(gly)_4^-$ at two different pH values, 6.8 and 7.5. We acquired BIRDS and CEST data at two different ambient temperatures, 30°C (Figure S2A-C) and 37°C (Figure S2E-G). For each sample, using Equation 4, we calculated average pH values of 6.72 ± 0.05 and 7.42 ± 0.06, respectively, at 30°C (Figure S2D), and 6.75 ± 0.04 and 7.58 ± 0.05, respectively, at 37°C (Figure S2H). These results demonstrate a good agreement between the pH values calculated using the ratiometric approach and those measured with the pH meter at both temperatures investigated, even at lower agent concentrations.

To demonstrate that the ratiometric approach proposed in this work can be applied successfully in vivo, we obtained BIRDS and CEST data in rat brains implanted with RG2 tumors (Figure 9). First, combined use of the paramagnetic agents TmDOTA-$(gly)_4^-$ and EuDOTA-$(gly)_4^-$ causes significant T_2 darkening to delineate the tumor boundary (Figure 9A). Second, Z-spectra of upfield/downfield peaks and CSI spectra for Tm-H2, Tm-H6, and Eu-H4 protons, from normal brain (Figure 9B) and tumor voxels (Figure 9C), show the pH dependence from the CEST peaks and T dependence from the proton chemical shifts. Notably, due to increased concentration of the agents inside the tumor compared with normal brain tissue, both CEST/BIRDS signals are much stronger in tumors, with SNR for in vivo CSI signals in the range 2 to 10. It is important to note that the in vivo detected CEST/BIRDS signals are in similar shift ranges as in in vitro data collected for physiological pH and T conditions. For example, one can compare Tm-H2, Tm-H6, and Eu-H4 in Figure 9B,C with Figure 2C for BIRDS data, or compare CEST upfield/downfield peaks in Figure 9B,C with Figure 3C,F for CEST data. Because the in vivo CEST peaks are small, Figure S3 shows zoomed-in views of the in vivo and in vitro comparison. The in vivo and in vitro signals of CEST/BIRDS look similar (differences of about 5%) because there are no endogenous pools so far downfield/upfield of water. The main distinction between the in vivo and in vitro data is that the former is slightly broader due to inhomogeneous distribution of agents within the voxels.

The ratiometric CEST measurements indicated a range of $CEST^{Tm/Eu}$ from 1.15 to 2.13 inside tumor with an average value of 1.8 ± 0.2, while for normal brain tissue a range of 2.2 to 3.5 with an average value of 2.56 ± 0.2 was measured (Figure 10A). Average temperatures of 35.3 ± 0.8 and 36.6 ± 0.6°C were measured inside the tumor and in normal tissue, respectively (Figure 10B). Using the ratiometric PARACEST calibrated with BIRDS (Equation 4), we measured an average pH value of 6.81 ± 0.08 inside tumor (Figure 10C), reflecting the acidity of the TME observed previously,[21,30] while the average pH for normal tissue was higher, 7.30 ± 0.06. Figure S4 illustrates the estimation of error maps in rat brains using the RMSD algorithm for R (Figure S4A), T (Figure S4B), and pH (Figure S4C). The results indicate that normal brain regions have higher deviations (errors) compared with tumor regions, most likely due to a lower agent concentration in these regions.

4 | DISCUSSION

Development of pH-imaging techniques with MRI or CSI at high resolution is necessary because pH deviations from neutral values are related to a variety of pathological diseases (e.g. cancer, stroke).[26,31–34] Quantitative pH imaging using conventional CEST is challenging because the CEST effect depends on a variety of factors including agent concentration, temperature, bulk water relaxation times, shimming (or B_0 field homogeneity) and RF intensity used for water saturation (or B_1 field). pH imaging using the ratiometric CEST technique was first introduced for concentration-

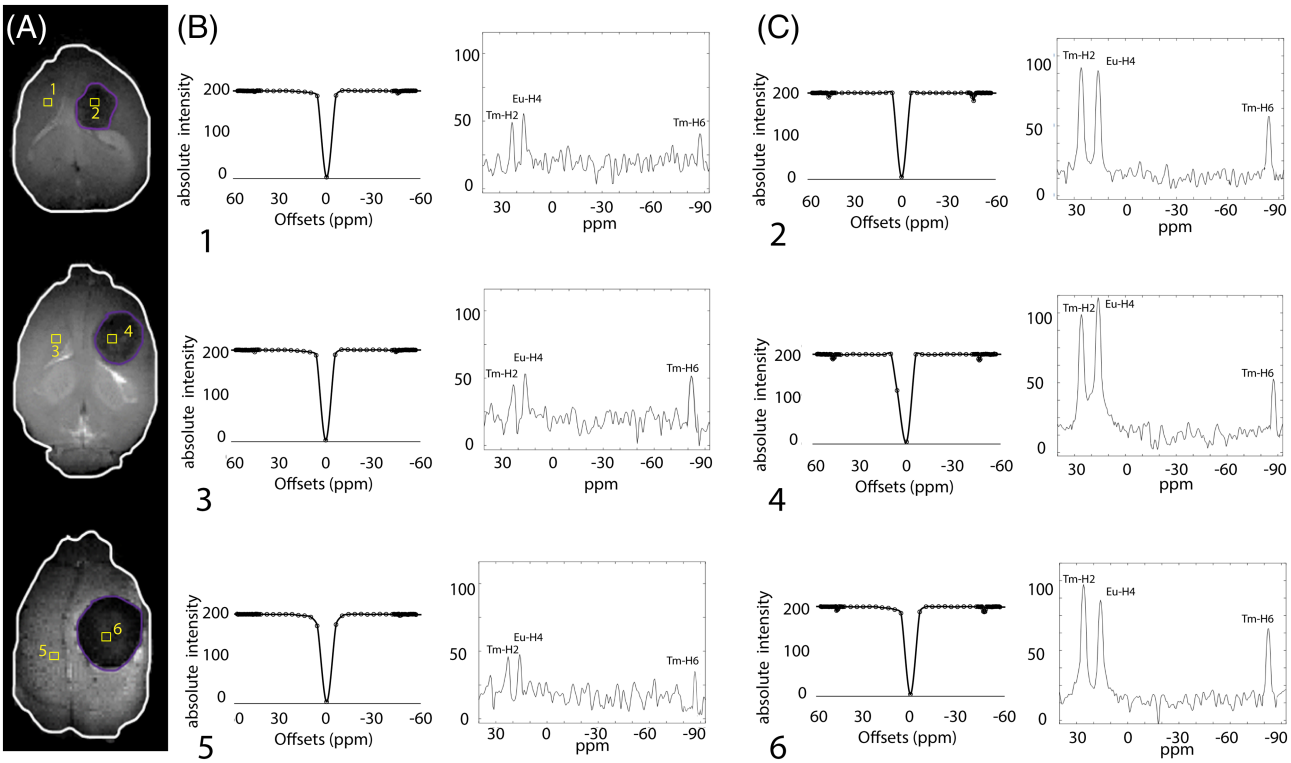

FIGURE 9 In vivo CEST and BIRDS using the EuDOTA-$(gly)_4^-$ and TmDOTA-$(gly)_4^-$ mixture in three rat brains with RG2 tumor. (A) The T_2-weighted images obtained after administration of paramagnetic agents, which can delineate the tumor boundary due to their extravasation (purple outline), where (B) voxels 1, 3, and 5 are in normal tissue and (C) voxels 2, 4, and 6 are in tumor tissue. The comparison of B and C shows the distinct upfield/downfield peaks for CEST (i.e. roughly around ±45 ppm) and BIRDS (i.e. Tm-H2, Tm-H6, and Eu-H4). The CEST/BIRDS peaks are much higher in the tumor regions. See Figure S3 for zoomed-in views of the upfield/downfield CEST peaks

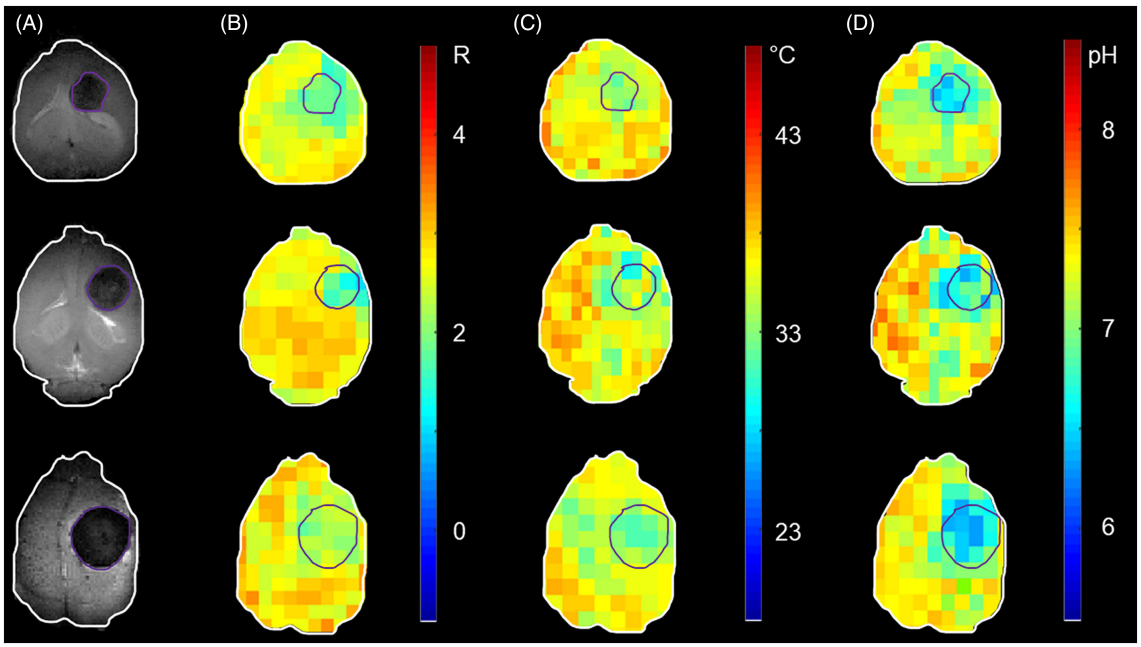

FIGURE 10 pH imaging at high resolution for three different rat brains with RG2 tumor using ratiometric CEST calibrated with BIRDS. (A) The tumor location (purple) on the anatomical MRI after the infusion of the EuDOTA-$(gly)_4^-$ and TmDOTA-$(gly)_4^-$ mixture. The next three columns show the (B) R (ratiometric CEST map), (C) T (temperature map from BIRDS), and (D) pH maps (from the BIRDS/CEST calibration using Equation 4). The pH in the tumor ranged from 6.4 to 6.9. See Figure S4 for estimated error maps for R, T, and pH

independent measurements using diamagnetic agents.[35] Subsequent pH-mapping studies using this ratiometric approach were based on either single PARACEST agents with multiple exchangeable pools, or multiple PARACEST agents.[36,37] In the present work we provide an improved ratiometric CEST approach, where temperature measurements with BIRDS using the same two agents are used to adjust the CEST intensity to account for temperature variations in the tissue microenvironment. Although this effect was thought to be small in vivo because the temperature variation across brain tissue does not usually exceed 1–2°C under normal experimental conditions,[16] this correction significantly improves the accuracy of pH measurement. For example, according to Equation 4, and assuming that we measured R to be 2.4 using CEST, the calculated pH would be 7.18 at a temperature of 35°C and 7.06 at a temperature of 36°C. This example shows that a temperature variation of 1°C could result in an error of 0.12 for the pH estimation. Therefore, accurate temperature measurements with BIRDS, for which the error in temperature determination is smaller than 0.1°C,[13,14] would significantly improve the accuracy of pH measurement using the CEST ratiometric approach.

The error in pH determination depends on the measurement uncertainty of the independent variables T and R, according to Equation 4. However, to calculate a pH error map, we need to use the error maps for T and R. The errors in T and R depend on the uncertainty in measuring the chemical shifts and CEST peak amplitudes, which should be considered for error estimation. In turn, the errors in T and R depend on contrast agents' concentrations and thus vary for different brain regions (e.g. tumors vs. normal tissue). For our in vivo measurements based on the RMSD algorithm (supporting information, appendix), we estimate an average error of 0.1°C for T and 0.15 for an R at 37°C and with R of 3.2. Using these values, the pH calculated using Equation 4 is 7.27 and the error for pH determination is 0.08.

Temperature determination with BIRDS is facilitated by the fact that the proton resonances in the mixture are well dispersed, with those of TmDOTA-$(gly)_4^-$ being shifted more than those of EuDOTA-$(gly)_4^-$ because the Tm^{3+} ion induces larger shifts than Eu^{3+} (Figure 2). The CEST signals of exchangeable protons were not observed with BIRDS under current experimental conditions (35°C and pH 7.4) because their chemical exchange rate was too fast, resulting in broadening of their corresponding resonances beyond detection. Mixing the TmDOTA-$(gly)_4^-$ and EuDOTA-$(gly)_4^-$ agents does not affect temperature determination with BIRDS, as demonstrated by identical chemical shifts measured in separate samples and in the mixture (Figure 3), and by a slope very close to unity obtained when plotting the temperature sensitivities C_T in separate samples and in the mixture for all protons (Figure 4). This allows the use of a mixture of two agents for our ratiometric CEST approach to ultimately provide pH mapping at high resolution. Moreover, using nonexchangeable signals from both agents improves the accuracy in temperature determination due to the added redundancies specific to the BIRDS approach.[13,17]

The amide protons in EuDOTA-$(gly)_4^-$ were not used in this study because their chemical shift is too close to water (Figure 3), and thus would have been affected by direct water saturation and magnetization transfer contributions. These effects are minimal for the other exchangeable pools of TmDOTA-$(gly)_4^-$ and EuDOTA-$(gly)_4^-$, which are about ±50 ppm removed from the bulk water pool. TmDOTA-$(gly)_4^-$ and EuDOTA-$(gly)_4^-$ were previously used individually for pH or temperature mapping.[10,15,38] The temperature sensitivities of amide protons in TmDOTA-$(gly)_4^-$ and of bound water in EuDOTA-$(gly)_4^-$ are in the same range as that of nonexchangeable protons used for BIRDS. However, these signals have lower sensitivity and require longer acquisition times for accurate temperature determination. Although CEST agents have shown their promise in pH and temperature mapping, using multiple agents (i.e. two in the present work) for quantitative pH imaging remains challenging due to their variable response to environmental changes. For example, in TmDOTA-$(gly)_4^-$ the CEST amplitude increases with temperature, while in EuDOTA-$(gly)_4^-$ it decreases, and the peak becomes broader (Figure 3). Proton relaxation times increase with temperature,[39] resulting in reduced widths of the observed CEST peaks. However, the major contribution to both peak broadening and amplitude changes of CEST peaks comes from the temperature dependence of chemical exchange rates.[40,41] The exchange of the amide protons of TmDOTA-$(gly)_4^-$ is slow and an increase in its exchange rate with temperature would bring the exchange regime towards a more optimal CEST effect (higher amplitude). The opposite effect is observed for the water molecule exchange in the EuDOTA-$(gly)_4^-$ complex, for which the exchange is most likely too fast for optimal CEST effect, and an increase in its exchange rate with temperature results in a decrease of its CEST amplitude.

DOTA-based PARACEST agents are commonly used for a variety of applications.[10,15,42] The CEST amplitude of the amide protons from TmDOTA-$(gly)_4^-$ is sensitive to pH changes, while that of the bound water protons from EuDOTA-$(gly)_4^-$ is less (Figure 3C). However, the ratio between the CEST amplitudes of these two signals in the mixture remains pH-sensitive, and in addition provides a measurable quantity that is concentration-independent. Because temperature also affects the exchange rates of exchangeable pools, and thus the CEST ratio for both TmDOTA-$(gly)_4^-$ and EuDOTA-$(gly)_4^-$ (Figure 3F), the dependence of the CEST ratio on pH is temperature-dependent (Figures 6 and 7). Therefore, to accurately determine the pH from the CEST ratio, we also need to measure the temperature independently. The advantage of using a mixture of TmDOTA-$(gly)_4^-$ and EuDOTA-$(gly)_4^-$ agents for pH determination is that it provides both the temperature readout with BIRDS and the CEST ratio. Moreover, although the two agents have different lanthanide ions, because they share the same DOTA-$(gly)_4^{4-}$ ligand, we expect that they will have a very similar spatial distribution not only in the brain, but also in other organs.

We have shown previously that BIRDS is a sensitive method for molecular imaging of pH and temperature.[13,17] Either TmDOTA-$(gly)_4^-$ or EuDOTA-$(gly)_4^-$ can serve as dual CEST/BIRDS agents. However, using a mixture of TmDOTA-$(gly)_4^-$ and EuDOTA-$(gly)_4^-$ allows us to use proton resonances from both agents to enhance the overall sensitivity and accuracy due to added redundancy. Using the chemical shift difference between the Tm-H2 and Tm-H6 resonances we achieve a temperature sensitivity of −0.74 ppm/°C, which is higher than the temperature sensitivities provided by either resonance alone (−0.25 and 0.48 ppm/°C for Tm-H2 and Tm-H6, respectively). This enhanced temperature sensitivity is due to shifting of these two resonances in opposite directions (from water) with temperature.

The combined BIRDS/CEST method for high-resolution in vivo pH imaging proposed in this work can be used for applications involving potential temperature variations present across brain regions in altered pathological states. A good example is longitudinal monitoring of therapeutic response during tumor treatment,[21,30] where we expect temperature differences between pathological and nonpathological tissue. We used the RG2 cell line for this work because it provides a simple and reproducible glioma model. The RG2 glioma has a highly invasive pattern of growth and mimics well the behavior of GBMs. Compared with other cell lines used to create GBM models, RG2 cultures reflect morphological homogeneity.[43,44] Because of these morphological characteristics, the BIRDS-measured pH maps of RG2 tumors look more homogeneous compared with tumor models derived from other cell lines like U87 and U251 tumors.[21,30,45] Measurements in rat brains implanted with RG2 gliomas using BIRDS indicate an average temperature of 35.3 ± 0.8°C inside the tumor, which was lower than the body temperature of 36.6 ± 0.6°C measured during the scan, similar to prior observations in anesthetized rat brain.[16] A slightly lower temperature was also measured inside the tumors compared with normal brain tissue (Figure 10). This result can be explained, according to analysis performed by Amri et al.[46] and Jiang et al.,[47] by a decreased rate of heat production in tumors compared with normal brain tissue. However, additional measurements are needed to better understand the relationship between blood flow, metabolism, and temperature inside tumors.

A limitation of the proposed method was the need to switch from a volume RF coil used for CEST (to provide a uniform B_1 saturation field) to a surface RF coil for BIRDS (to provide a better SNR). To address this limitation in the future, both CEST and BIRDS datasets could be acquired using the same RF coil with a specific geometry (e.g. saddle shape), which could provide both a more uniform B_1 saturation and high SNR. Another limitation is the use of a mixture of two paramagnetic contrast agents, which is not a very common procedure, especially under clinical settings. However, this hybrid CEST/BIRDS method can be applied using a single contrast agent, provided that the agent has two different exchangeable pools and temperature- (or pH-) sensitive BIRDS peaks.

In conclusion, we developed a high-resolution pH-imaging technique involving a combination of BIRDS and CEST detections using a mixture of two paramagnetic agents, TmDOTA-$(gly)_4^-$ and EuDOTA-$(gly)_4^-$. Our ratiometric CEST results indicate that accurate pH determination in vivo requires an additional temperature measurement with BIRDS.

ACKNOWLEDGMENTS

We acknowledge the technical support of the staff within the Yale MRRC for assistance with animal care. This study was supported by NIH grant R01 EB-023366. JJW was supported in part by T32 GM-007205.

CONFLICT OF INTEREST

All the authors declare no conflict of interest.

DATA AVAILABILITY STATEMENT

The data that support the findings of this study are available from the corresponding author upon reasonable request.

ORCID

Daniel Coman https://orcid.org/0000-0002-6289-0817

REFERENCES

1. Kubíček V, Tóth É. Design and function of metal complexes as contrast agents in MRI. In: van Eldik R, Hubbard CD, eds. *Advances in Inorganic Chemistry*. Vol. 61. Cambridge Massachusetts: Academic Press; 2009:63-129.
2. Viswanathan S, Kovacs Z, Green KN, Ratnakar SJ, Sherry AD. Alternatives to gadolinium-based MRI metal chelates. *Chem Rev*. 2010;110(5):2960-3018.
3. Sherry AD, Woods M. Chemical exchange saturation transfer contrast agents for magnetic resonance imaging. *Annu Rev Biomed Eng*. 2008;10:391-411.
4. van Zijl PCM, Yadav NN. Chemical exchange saturation transfer (CEST): What is in a name and what isn't? *Magn Reson Med*. 2011;65(4):927-948.
5. Dorazio SJ, Olatunde AO, Tsitovich PB, Morrow JR. Comparison of divalent transition metal ion paraCEST MRI contrast agents. *J Biol Inorg Chem*. 2014;19(2):191-205.
6. Evbuomwan OM, Terreno E, Aime S, Sherry AD. CEST and PARACEST agents for molecular imaging. In: *The Chemistry of Molecular Imaging*. New Jersy, United States: John Wiley & Sons, Ltd; 2014:225-243.
7. Woods M, Woessner DE, Sherry AD. Paramagnetic lanthanide complexes as PARACEST agents for medical imaging. *Chem Soc Rev*. 2006;35(6):500-511.
8. Aime S, Castelli DD, Crich SG, Gianolio E, Terreno E. Pushing the sensitivity envelope of lanthanide-based magnetic resonance imaging (MRI) contrast agents for molecular imaging applications. *Acc Chem Res*. 2009;42(7):822-831.
9. Aime S, Barge A, Delli Castelli D, et al. Paramagnetic lanthanide (III) complexes as pH-sensitive chemical exchange saturation transfer (CEST) contrast agents for MRI applications. *Magn Reson Med*. 2002;47(4):639-648.
10. Aime S, Delli Castelli D, Terreno E. Novel pH-reporter MRI contrast agents. *Angew Chem Int Ed Engl*. 2002;41(22):4334-4336.
11. Wu Y, Soesbe TC, Kiefer GE, Zhao P, Sherry AD. A responsive europium (III) chelate that provides a direct readout of pH by MRI. *J Am Chem Soc*. 2010;132(40):14002-14003.

12. Woessner DE, Zhang S, Merritt ME, Sherry AD. Numerical solution of the Bloch equations provides insights into the optimum design of PARACEST agents for MRI. *Magn Reson Med.* 2005;53(4):790-799.
13. Coman D, Trubel HK, Rycyna RE, Hyder F. Brain temperature and pH measured by 1H chemical shift imaging of a thulium agent. *NMR Biomed.* 2009; 22(2):229-239.
14. Coman D, Trubel HK, Hyder F. Brain temperature by biosensor imaging of redundant deviation in shifts (BIRDS): comparison between TmDOTP5− and TmDOTMA−. *NMR Biomed.* 2010;23(3):277-285.
15. Coman D, Kiefer GE, Rothman DL, Sherry AD, Hyder F. A lanthanide complex with dual biosensing properties: CEST and BIRDS with EuDOTA-(gly) 4−. *NMR Biomed.* 2011;24(10):1216-1225.
16. Coman D, de Graaf RA, Rothman DL, Hyder F. In vivo 3D molecular imaging with BIRDS at high spatiotemporal resolution. *NMR Biomed.* 2013;26(11): 1589-1595.
17. Coman D, Sanganahalli BG, Jiang L, Hyder F, Behar KL. Distribution of temperature changes and neurovascular coupling in rat brain following 3,4-methylenedioxymethamphetamine (MDMA, "ecstasy") exposure. *NMR Biomed.* 2015;28(10):1257-1266.
18. Huang Y, Coman D, Ali MM, Hyder F. Lanthanide ion (III) complexes of 1,4,7,10-tetraazacyclododecane-1,4,7,10-tetraaminophosphonate (DOTA-4AmP8−) for dual biosensing of pH with CEST (chemical exchange saturation transfer) and BIRDS (biosensor imaging of redundant deviation in shifts). *Contrast Media Mol Imaging.* 2015;10(1):51-58.
19. Huang Y, Coman D, Hyder F, Ali MM. Dendrimer-based responsive MRI contrast agents (G1-G4) for biosensor imaging of redundant deviation in shifts (BIRDS). *Bioconjug Chem.* 2015;26(12):2315-2323.
20. Walsh JJ, Huang Y, Simmons JW, et al. Dynamic thermal mapping of localized therapeutic hypothermia in the brain. *J Neurotrauma.* 2020;37(1):55-65.
21. Coman D, Huang Y, Rao JU, et al. Imaging the intratumoral-peritumoral extracellular pH gradient of gliomas. *NMR Biomed.* 2016;29(3):309-319.
22. Gatenby RA, Gillies RJ. Why do cancers have high aerobic glycolysis? *Nat Rev Cancer.* 2004;4(11):891-899.
23. Warburg O. On the origin of cancer cells. *Science.* 1956;123(3191):309-314.
24. Gillies RJ, Raghunand N, Garcia-Martin ML, Gatenby RA. pH imaging. A review of pH measurement methods and applications in cancers. *IEEE Eng Med Biol Mag.* 2004;23(5):57-64.
25. Raghunand N. Tissue pH measurement by magnetic resonance spectroscopy and imaging. *Methods Mol Med.* 2006;124:347-364.
26. Longo DL, Sun PZ, Consolino L, Michelotti FC, Uggeri F, Aime S. A general MRI-CEST ratiometric approach for pH imaging: demonstration of in vivo pH mapping with iobitridol. *J Am Chem Soc.* 2014;136(41):14333-14336.
27. Bertini I, Luchinat C, Parigi G, Pierattelli R. NMR spectroscopy of paramagnetic metalloproteins. *Chembiochem.* 2005;6(9):1536-1549.
28. Wang Z, Bovik AC, Sheikh HR, Simoncelli EP. Image quality assessment: from error measurement to structural similarity. *IEEE Trans Image Process.* 2004;13:14-612.
29. Zhang S, Sherry AD. Physical characteristics of lanthanide complexes that act as magnetization transfer (MT) contrast agents. *J Solid State Chem.* 2003;171(1–2):38-43.
30. Huang Y, Coman D, Herman P, Rao JU, Maritim S, Hyder F. Towards longitudinal mapping of extracellular pH in gliomas. *NMR Biomed.* 2016;29(10): 1364-1372.
31. Chen LQ, Pagel MD. Evaluating pH in the extracellular tumor microenvironment using CEST MRI and other imaging methods. *Adv Radiol.* 2015;2015: 206405.
32. Liu H, Jablonska A, Li Y, et al. Label-free CEST MRI detection of citicoline-liposome drug delivery in ischemic stroke. *Theranostics.* 2016;6(10):1588-1600.
33. McVicar N, Li AX, Gonçalves DF, et al. Quantitative tissue pH measurement during cerebral ischemia using amine and amide concentration-independent detection (AACID) with MRI. *J Cereb Blood Flow Metab.* 2014;34(4):690-698.
34. Sun PZ, Wang E, Cheung JS, Zhang X, Benner T, Sorensen AG. Simulation and optimization of pulsed radio frequency (RF) irradiation scheme for chemical exchange saturation transfer (CEST) MRI – demonstration of pH-weighted pulsed-amide proton CEST MRI in an animal model of acute cerebral ischemia. *Magn Reson Med.* 2011;66(4):1042-1048.
35. Ward KM, Balaban RS. Determination of pH using water protons and chemical exchange dependent saturation transfer (CEST). *Magn Reson Med.* 2000;44(5):799-802.
36. Delli Castelli D, Terreno E, Aime S. Yb (III)-HPDO3A: a dual pH- and temperature-responsive CEST agent. *Angew Chem Int Ed Engl.* 2011;50(8):1798-1800.
37. Rancan G, Delli Castelli D, Aime S. MRI CEST at 1T with large μeff Ln(3+) complexes T m(3+)-HPDO3A: An efficient MRI pH reporter. *Magn Reson Med.* 2016;75(1):329-336.
38. Zhang S, Malloy CR, Sherry AD. MRI thermometry based on PARACEST agents. *J Am Chem Soc.* 2005;127(50):17572-17573.
39. Kamman RL, Go KG, Brouwer W, Berendsen HJ. Nuclear magnetic resonance relaxation in experimental brain edema: effects of water concentration, protein concentration, and temperature. *Magn Reson Med.* 1988;6(3):265-274.
40. Wu Y, Zhang S, Soesbe TC, et al. pH imaging of mouse kidneys in vivo using a frequency-dependent paraCEST agent. *Magn Reson Med.* 2016;75(6): 2432-2441.
41. Evbuomwan OM, Lee J, Woods M, Sherry AD. The presence of fast-exchanging proton species in aqueous solutions of paraCEST agents can impact rate constants measured for slower exchanging species when fitting CEST spectra to the Bloch equations. *Inorg Chem.* 2014;53(19):10012-10014.
42. Opina ACL, Wu Y, Zhao P, Kiefer G, Sherry AD. The pH sensitivity of −NH exchange in LnDOTA-tetraamide complexes varies with amide substituent. *Contrast Media Mol Imaging.* 2011;6(6):459-464.
43. Ko L, Koestner A, Wechsler W. Morphological characterization of nitrosourea-induced glioma cell lines and clones. *Acta Neuropathol.* 1980;51(1): 23-31.
44. Barth RF, Kaur B. Rat brain tumor models in experimental neuro-oncology: the C6, 9L, T9, RG2, F98, BT4C, RT-2 and CNS-1 gliomas. *J Neurooncol.* 2009;94(3):299-312.
45. Rao JU, Coman D, Walsh JJ, Ali MM, Huang Y, Hyder F. Temozolomide arrests glioma growth and normalizes intratumoral extracellular pH. *Sci Rep.* 2017;7:7865.
46. Amri A, Saidane A, Pulko S. Thermal analysis of a three-dimensional breast model with embedded tumour using the transmission line matrix (TLM) method. *Comput Biol Med.* 2011;41(2):76-86.

47. Jiang L, Zhan W, Loew MH. Modeling static and dynamic thermography of the human breast under elastic deformation. *Phys Med Biol*. 2010;56(1): 187-202.

SUPPORTING INFORMATION

Additional supporting information may be found in the online version of the article at the publisher's website.

How to cite this article: Mihailovic JM, Huang Y, Walsh JJ, et al. High-resolution pH imaging using ratiometric chemical exchange saturation transfer combined with biosensor imaging of redundant deviation in shifts featuring paramagnetic DOTA-tetraglycinate agents. *NMR in Biomedicine*. 2022;35(5):e4658. doi:10.1002/nbm.4658